

Effect of 2D Velocity Profiles on Optical Measurements

Nicholas Tapias

University of Washington
Department of Chemical Engineering

June 1, 2006

Microfluidic devices involve fluid flow through channels at flow rates that are not easily measured using conventional techniques. Typically the only way to access the dimensions of the channel is using optics. The ultimate goal is to develop generalized charts that can be used to characterize fluid flow through rectangular microchannels of various aspect ratios and boundary conditions using the Poisson equation (Equation 1). The Poisson equation relates the velocity distribution in a space where the pressure drop, viscosity and path length are known.

Equation 1 – Poisson Equation

$$\nabla^2 u = \frac{\Delta p}{\mu L}$$

For the purposes of these calculations, the quantity $\frac{\Delta p}{\mu L}$ was assigned as unity. The physical dimensions of the microchannels investigated in this research are listed in Table 1.

Table 1 – Physical properties

<i>Closed Channel</i>			<i>Open Channel</i>		
Aspect Ratio	Width (μm)	Height (μm)	Aspect Ratio	Width (μm)	Height (μm)
1:1	1	1	1:1	1	1
1:2	2	1	1:2	2	1
1:3	3	1	1:3	3	1
1:4	4	1	1:4	4	1
1:5	5	1	1:5	5	1
1:6	6	1	1:6	6	1

The depth of each channel was defined as 1μ and the width was varied dependent upon the aspect ratio investigated. An important part of this experiment was to compare the flow through closed and open channel conditions. Figure 1 illustrates the boundary conditions used for each closed and open channel arrangement. No-slip boundary conditions were imposed upon the entire exterior boundary of the closed channel arrangements. Open channel arrangements were modified with a slip or symmetry boundary at the top of the channel, allowing for the fluid to flow freely at this boundary. As indicated in the figure symmetry was used to simplify the calculation and increase the accuracy of the calculation using the finite element software. Another consequence of this symmetry is the repetition of measurements. One such repetition is that of an open

channel 1:2 being also representative of a closed channel 1:1. The slip boundary at the top in such an open channel is equivalent to a symmetric line that divides such a 1:1 channel, but for the purposes of this research it is important to consider each case separately, as the fraction of the total flow for each subdomain is different as the boundary condition is altered. A slip or symmetry boundary was placed at the midpoint across the channel since we know that the flow characteristics of the right side will be a reflection of the left side.

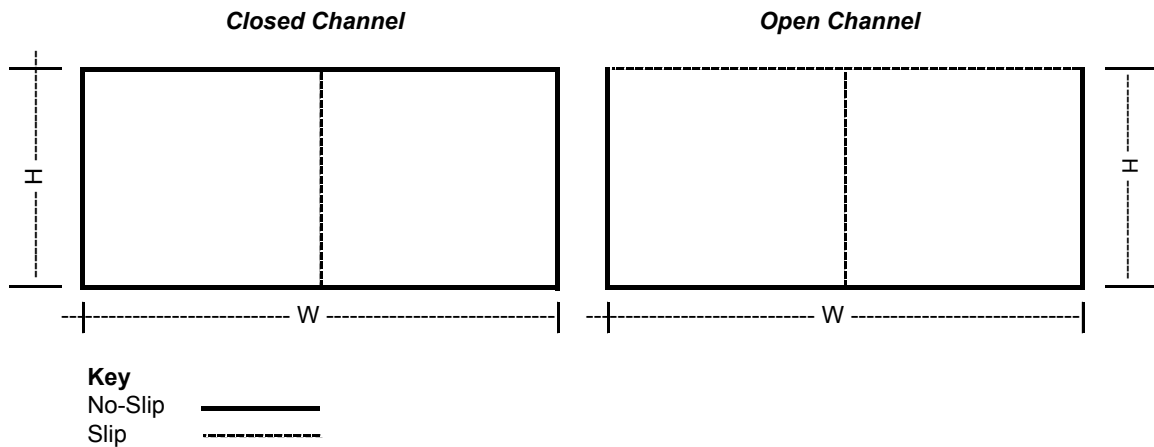


Table 2 – Solution characteristics
Closed Channel

Aspect Ratio	Elements	DOF
1:1	217216	436561
1:2	62368	125849
1:3	232768	467737
1:4	229440	461145
1:5	230208	462697
1:6	227712	457713

Open Channel

Aspect Ratio	Elements	DOF
1:1	217216	436561
1:2	249472	501169
1:3	232768	467737
1:4	229440	461145
1:5	230208	462697
1:6	227712	457713

The flow through each subdomain of the channel was evaluated using subdomain integration in FEMLAB. Equation 2 below shows the relation between velocity and flow rate.

Equation 2

$$V(x) = \int u \, dA$$

The size of each subdomain varied across the whole domain. The width of the subdomains near the edge was approximately 4 nm wide. The largest subdomain examined was 0.3 μm . The lines visible in Figure 2 show the relative size of each examined subdomains for the 1:6 configuration channel. Additional variability in the dimensions of the larger elements of the domain was included to ensure that measurements were representative of the actual flow profile through the channel. This can be seen in the figure as well, as each subdomain on the right side of the figure is not identical to the previous one. Having this variability also ensures that the placement of elements within the domain are equally distributed and that accuracy of the measurement is not restricted only to the very small subdomains.

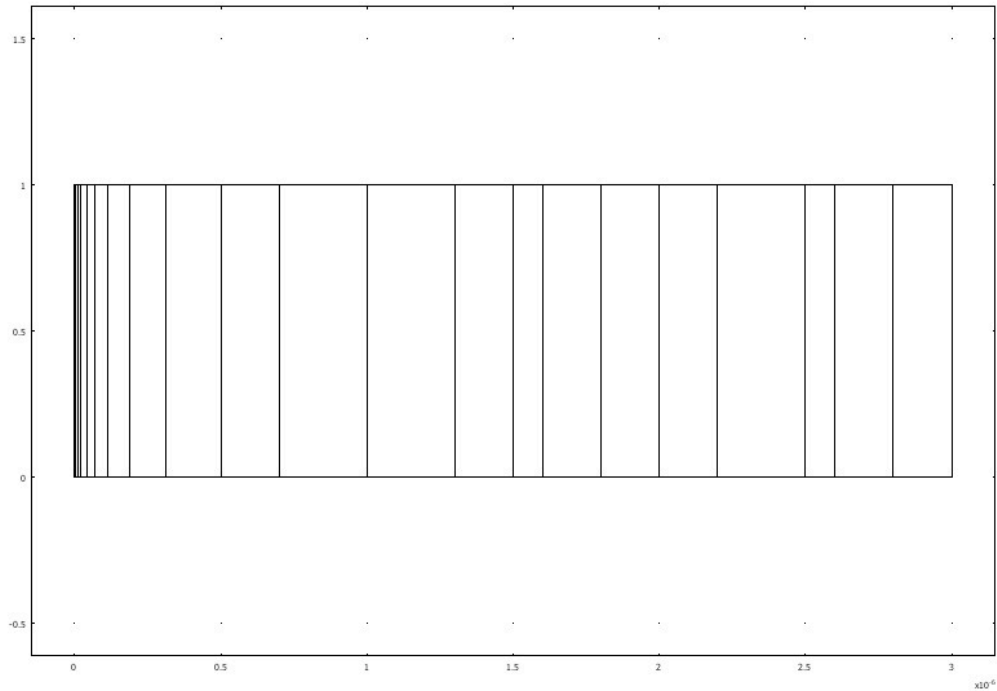


Figure 2 – Illustration of subdomains in the 1:6 channel

Each subdomain was established as a neutral boundary to prevent any interaction with the simulated fluid within the channel. By dividing the channel into subdomains, it was possible to evaluate over a finite portion of the channel. Figure 3 below shows a color surface of the velocity profile in the closed and open channel geometries. The example shown is for a 1:3 aspect ratio. Important to note is that only the left half of channel was modeled to permit for more precise elements in the portions near the left.

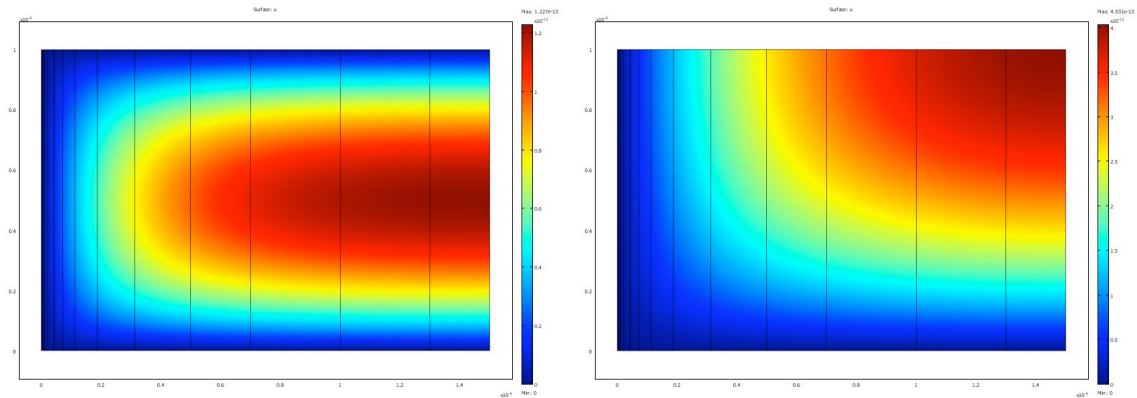


Figure 3 - Velocity surfaces for 1:3 configuration, closed channel (left) and open channel (right)

Using this result and equation 2 it was possible to evaluate the flow rate through each of the subdomains. Figures 4 and 5 show the cumulative flow fraction for the closed and open channel geometries

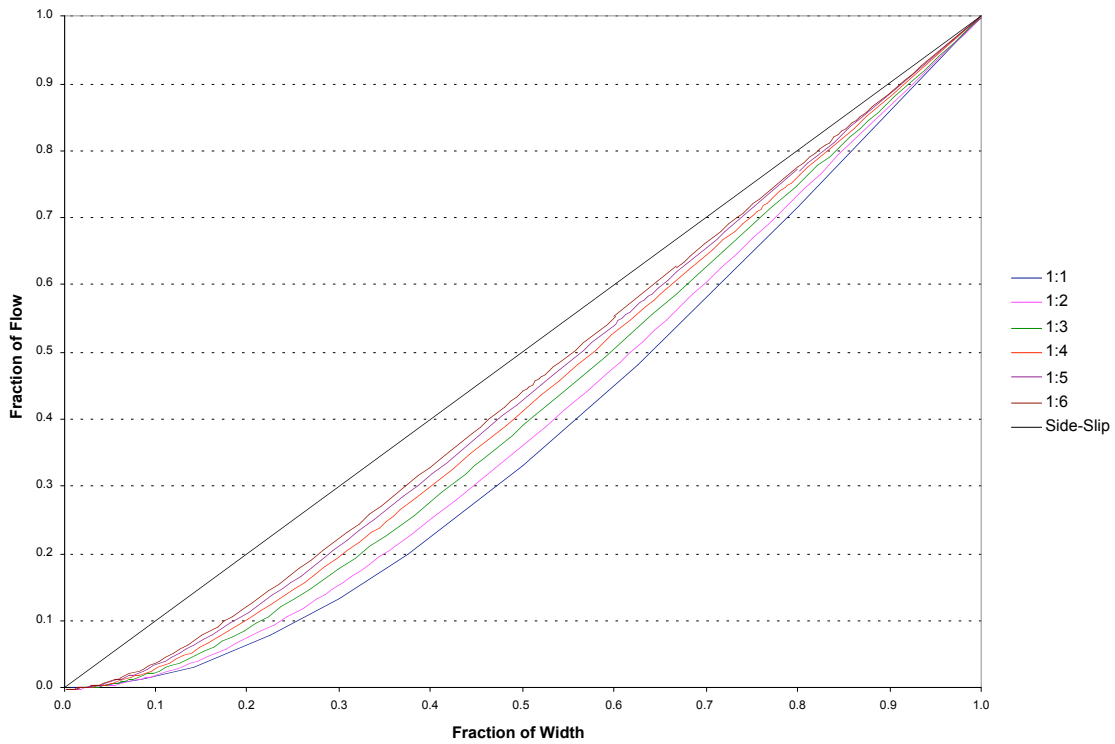


Figure 4 – Closed Channel: Fraction of total width vs. Fraction of total flow

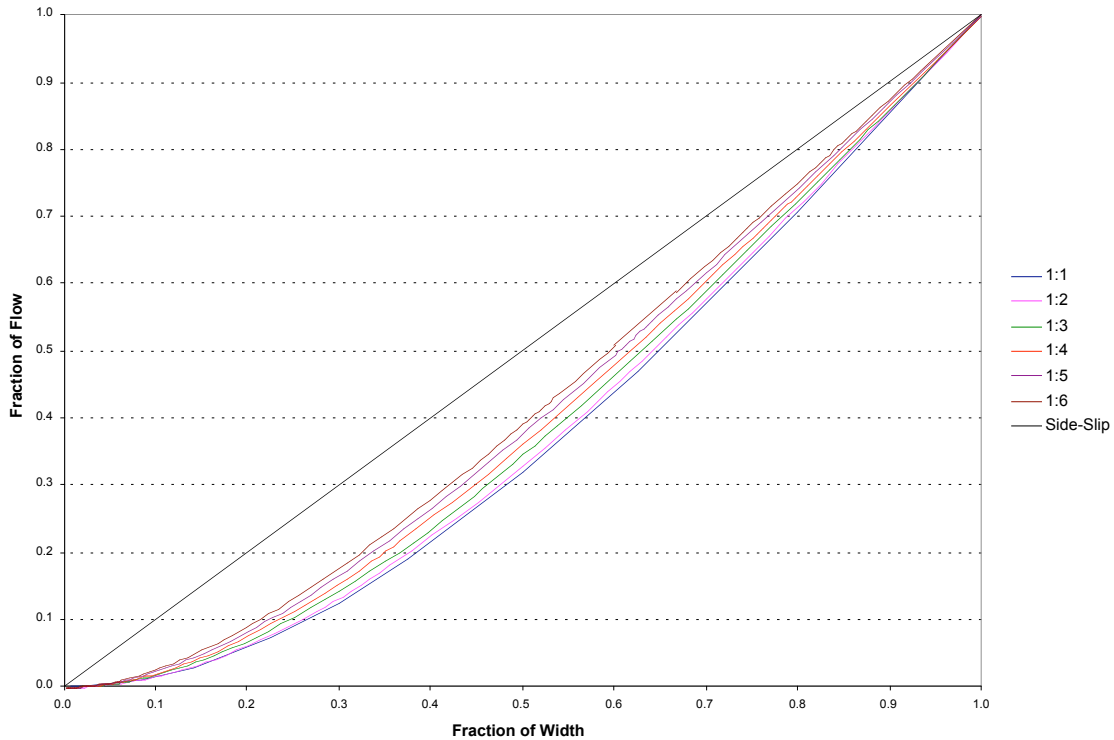


Figure 5 – Open Channel: Fraction of total width vs. Fraction of total flow

Some important flow characteristics can be seen in these two generalized charts. The linear behavior of the flow accumulation after approximately 1/3 of the channel width is realized. This can be interpreted to represent that the vertical velocity profile after this point is constant. Also important to note from these generalized correlations is the variation near the no-slip boundary. The fraction of flow near the edge is significantly different for the different aspect ratios investigated.

Also shown on the plots are the conditions where the side walls of the channel were not designated as no-slip boundaries. This result would be representative of the flow for a channel with infinite width. The charts indicate that the fraction of flow to a specific width in the channel. Tables 3 and 4 show the third-order correlations of the fractional flow and the fractional width. Also shown are the R^2 values that were calculated. Each of these correlations were restricted to have zero flow at the left boundary ($u(x=0) = 0$).

Table 3 – Closed Channel flow fraction correlations

Aspect Ratio		R²
1:1	$y = -0.5634x^3 + 1.5283x^2 + 0.0344x$	1
1:2	$y = -0.6889x^3 + 1.598x^2 + 0.0901x$	0.9999
1:3	$y = -0.7337x^3 + 1.5484x^2 + 0.1806x$	0.9998
1:4	$y = -0.707x^3 + 1.426x^2 + 0.2742x$	0.9997
1:5	$y = -0.6977x^3 + 1.3427x^2 + 0.3468x$	0.9996
1:6	$y = -0.6633x^3 + 1.2346x^2 + 0.4182x$	0.9995

Table 4 – Open Channel flow correlations

Aspect Ratio		R²
1:1	$y = -0.5224x^3 + 1.5104x^2 + 0.0118x$	1
1:2	$y = -0.5729x^3 + 1.5437x^2 + 0.0289x$	1
1:3	$y = -0.6189x^3 + 1.5534x^2 + 0.0635x$	1
1:4	$y = -0.6497x^3 + 1.5388x^2 + 0.1075x$	0.9999
1:5	$y = -0.6916x^3 + 1.5375x^2 + 0.149x$	0.9999
1:6	$y = -0.7132x^3 + 1.5083x^2 + 0.1973x$	0.9998

Using these correlations it is possible to calculate the fractional flow that is contained within a specific portion of the channel of interest. An important result of this as well is that channels with aspect ratios less than 1:4 have a rapidly changing velocity profile near the fixed edges, whereas those with larger aspect ratios exhibit constant velocity profiles after the 1:4 aspect ratio has been realized. Figure 6 below further illustrates this case in 1:12 aspect ratio channels.

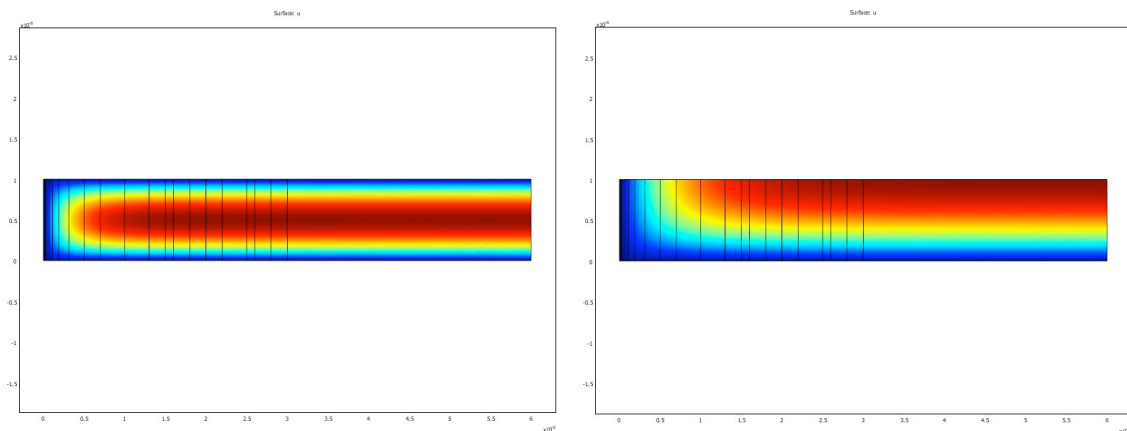


Figure 6 – Flow through 1:12 aspect ratio channels

These linear profiles allows for easier determination of the flow rate through the channels. Because the flow is then simply a function of the width of interest, the cumulative flow rate will be a linear profile. The width necessary for each aspect ratio to recover this linear velocity profile was determined analytically by satisfying the condition expressed in Equation 3.

Equation 3

$$\nabla^2 V(x) = 0$$

This condition states that at the point where the velocity profile stops changing in the x-direction along the channel, the flow rate as well should not be changing. This condition was then applied to the correlations obtained for fractional flow through the microchannels. Figure 7 illustrates how the fractional width along the channel for each aspect ratio to recover this linear velocity profile.

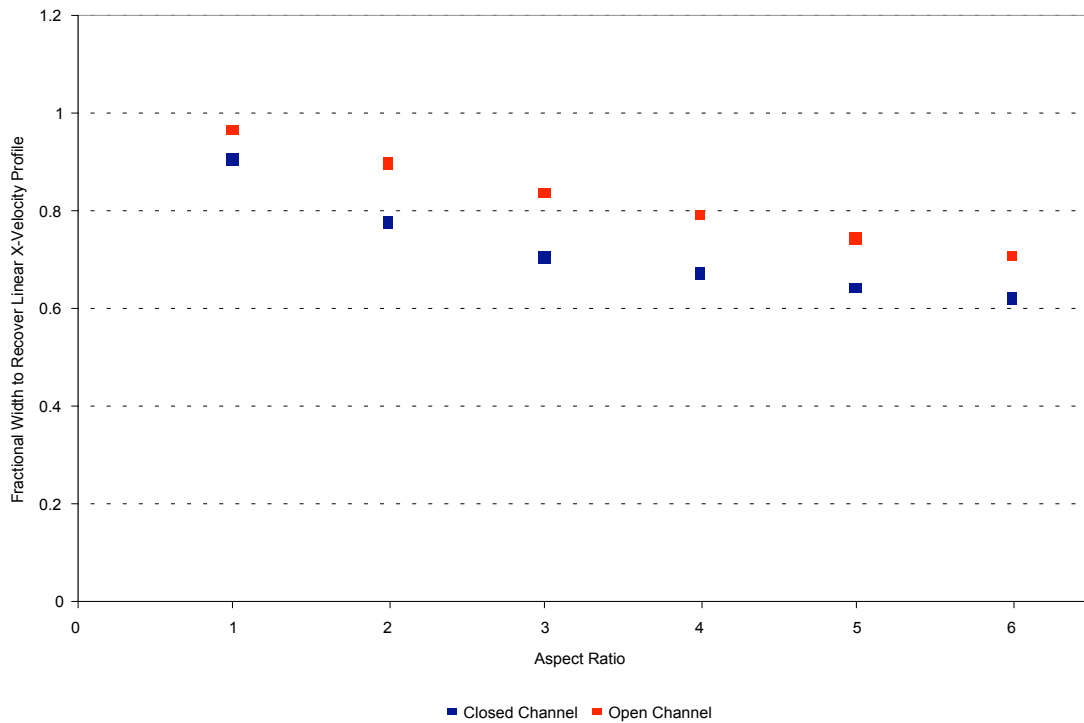


Figure 7 – Fractional width to recover linear x-velocity profile

These results can then be applied to determine the physical scale of these fractional widths. Table 5 below shows that as the aspect ratio increases, the linear velocity profile is recovered further in the x-direction than for smaller channels. An important result of this is that for different aspect ratios, the fraction to recover the linear velocity profile is different. As the channel widens a larger portion of the total flow is considered in the region of constant x-velocity.

Table 5 – Width to recover linear velocity profile

<i>Closed Channel</i>		<i>Open Channel</i>	
Aspect Ratio	Width (μm)	Aspect Ratio	Width (μm)
1:1	0.452	1:1	0.482
1:2	0.773	1:2	0.898
1:3	1.055	1:3	1.255
1:4	1.345	1:4	1.579
1:5	1.604	1:5	1.853
1:6	1.861	1:6	2.115

Also worth noting is that it requires more length along the x-direction to establish the linear x-velocity profile for the open channel than for the closed channel for all scenarios investigated. These results could be used to find the proper site to find the mean flow rate along the length of the channel.